JGR Solid Earth

RESEARCH ARTICLE
10.1029/2021JB023351

Mantle Viscosity Derived From Geoid and Different Land Uplift Data in Greenland

Mohammad Bagherbandi[1,2], Hadi Amin[1], Linsong Wang[3,4], and Masoud Shirazian[5]

[1]Department of Computer and Spatial Sciences, University of Gävle, Gävle, Sweden, [2]Division of Geodesy and Satellite Positioning, Royal Institute of Technology (KTH), Stockholm, Sweden, [3]Hubei Subsurface Multi-scale Imaging Key Laboratory, Institute of Geophysics and Geomatics, China University of Geosciences, Wuhan, China, [4]Helmholtz Centre Potsdam, GFZ German Research Centre for Geosciences, Telegrafenberg, Germany, [5]Department of Geomatics Engineering, Civil Engineering Faculty, Shahid Rajaee Teacher Training University, Tehran, Iran

Abstract The Earth's mass redistribution due to deglaciation and recent ice sheet melting causes changes in the Earth's gravity field and vertical land motion in Greenland. The changes are because of ongoing mass redistribution and related elastic (on a short time scale) and viscoelastic (on time scales of a few thousands of years) responses. These signatures can be used to determine the mantle viscosity. In this study, we infer the mantle viscosity associated with the glacial isostatic adjustment (GIA) and long-wavelength geoid beneath the Greenland lithosphere. The viscosity is determined based on a spatio-spectral analysis of the Earth's gravity field and the land uplift rate in order to find the GIA-related gravity field. We used different land uplift data, that is, the vertical land motions obtained by the Greenland Global Positioning System (GPS) Network (GNET), gravity recovery and climate experiment (GRACE) and glacial isostatic adjustment (GIA) data, and also combined them using the Kalman filtering technique. Using different land uplift rates, one can obtain different GIA-related gravity fields. As shown in this study, the mantle viscosities of 1.9×10^{22} Pa s and 7.8×10^{21} Pa s for a depth of 200–700 km are obtained using ICE-6G (VM5a) model and the combined land uplift model, respectively, and the GIA-related gravity potential signal.

Plain Language Summary The Earth is not a rigid object and has different dynamic changes that shape its mantle and surface. The heat of the Earth's core results in mantle flow, generating global mantle convection. The pressure of these flows pushes or pull the surface away from its isostatic equilibrium. Computing these stresses helps us have a better vertical land motion model for the Earth's surface. Another dynamic process that is important to include is glacial isostatic adjustment (GIA), an important issue for example, for the sea-level rise studies. The Earth's surface has not yet reached its equilibrium state due to the presence of huge ice sheets in the last 25,000 years. This crustal land uplift needs to be identified and modeled well. A gravimetric land uplift model was developed based on satellite gravity missions (GRACE recovery and climate experiment) and compared with the one obtained from the Global Positioning System data and geophysical models in this study. These data were used for determining the mantle viscosity in Greenland. The mantle viscosity models help us understand the mantle's mechanical behavior and the Earth's internal structure for example, the internal friction of the mantle flow and continental drift modeling.

Key Points:

- The upper mantle viscosity is determined using the glacial isostatic adjustment (GIA) related gravity field and land uplift rate in Greenland
- The gravity field signal related to the GIA is estimated by comparing the geoid and land uplift rate
- A combined land uplift rate using Global Positioning System, GRACE data recovery and climate experiment and GIA models is calculated using the Kalman filtering approach

Supporting Information:

Supporting Information may be found in the online version of this article.

Correspondence to:

M. Bagherbandi,
mohammad.bagherbandi@hig.se

Citation:

Bagherbandi, M., Amin, H., Wang, L., & Shirazian, M. (2022). Mantle viscosity derived from geoid and different land uplift data in Greenland. *Journal of Geophysical Research: Solid Earth*, *127*, e2021JB023351. https://doi.org/10.1029/2021JB023351

Received 3 OCT 2021
Accepted 28 JUL 2022

Author Contributions:

Conceptualization: Mohammad Bagherbandi
Data curation: Linsong Wang
Formal analysis: Mohammad Bagherbandi, Hadi Amin, Linsong Wang, Masoud Shirazian
Investigation: Mohammad Bagherbandi, Hadi Amin, Linsong Wang, Masoud Shirazian
Methodology: Mohammad Bagherbandi, Linsong Wang, Masoud Shirazian
Software: Mohammad Bagherbandi, Hadi Amin, Linsong Wang

1. Introduction

Glacial isostatic adjustment (GIA) describes the tendency of the Earth's crust to preserve lithospheric isostatic equilibrium when ice sheets load the crust. By analyzing the ongoing crustal rebound (adjustment), various phenomena can be studied, such as the rheological properties of the Earth's interior. The thermal and chemical heterogeneities within the mantle show that the mantle is a dynamic system. Therefore, there is a flow in the mantle which depends on the mantle rheology. Kaufmann & Lambeck (2000) discussed different mantle systems in their publication. They mentioned that the mantle could have different behaviors. In other words, the Earth's mantle can be described as an elastic (assuming short time scale), viscoelastic (few thousands of years' scale), and highly viscous (very long time scale) continua. It is essential to distinguish between the elastic and non-elastic behaviors of the mantle, especially for predicting the signatures related to the glacial isostatic adjustment process and estimating a model for the radial variation of mantle viscosity (Kaufmann & Lambeck, 2000). The signatures such as relative sea-level changes and changes in the Earth's gravitational field can be used to constrain the radial viscosity profile (Haskell, 1935). Many scholars have proposed different approaches to infer the mantle viscosity

Supervision: Mohammad Bagherbandi
Validation: Mohammad Bagherbandi, Hadi Amin, Linsong Wang, Masoud Shirazian
Writing – original draft: Mohammad Bagherbandi
Writing – review & editing: Mohammad Bagherbandi, Hadi Amin, Linsong Wang, Masoud Shirazian

after Haskell (1935) such as (Cathles III, 1975; Mitrovica & Forte, 2004; Paulson et al., 2007; Tushingham & Peltier, 1992; W. Richard Peltier, 1996; W. R Peltier & Andrews, 1976). An interesting comparison between different mantle viscosity modeling can be seen in Kaufmann and Lambeck (2000), where uniform and glacially induced viscosity models are compared. The comparison shows that the glacially induced viscosity models generally agree with the radial viscosity variations obtained from the mantle circulation (or flow) models. In another study, Tosi et al. (2005) showed that it is possible to use long-wavelength and time-dependent zonal components of the gravity field to constrain the mantle viscosity because the variation in the gravity field originates from the Earth's mass redistribution. Zhao et al. (2012) studied the lithospheric thickness and mantle viscosity using the inversion method and the GNSS solutions of the BIFROST project (cf. Johansson et al., 2002; Lidberg et al., 2010). They estimated the earth model parameters from inversion of the GNSS-derived horizontal and vertical displacements and also using a joint inversion by employing the two ice models (i.e., ANU-ICE and ICE-5G, see more in Lambeck et al. (2010) and W Richard Peltier (2004)). They also showed that the GPS data are best fit to a three-layer earth model and to estimate lithosphere thickness and mantle viscosity.

In this study, we follow the approach proposed by Bjerhammar et al. (1980) and Sjöberg and Bagherbandi (2013) to determine the mantle viscosity in Greenland. Here we use the long-wavelength geoid model and land uplift rates as input data. The GIA-related gravity signal should be precisely extracted from the geoid model. It has been shown that the GIA-related gravity signal has a long-wavelength characteristic (Bjerhammar et al., 1980; Hager & Richards, 1989; Simons & Hager, 1997; Sjöberg & Bagherbandi, 2013). Hence, the GIA-related gravity field (or geoid depression) can be used to model the mantle parameters for example, viscosity. Therefore, a spatiospectral method (i.e., correlation analysis) can be used for extracting the long-wavelength gravity field signal due to the GIA (Bjerhammar et al., 1980; Joud, 2018; Sjöberg & Bagherbandi, 2013). However, some of the previous viscosity inversion methods used harmonic windows of the gravity field more or less uncritically or based on earlier experiments in modeling the GIA-related gravity signals (e.g., Balling, 1980; Mitrovica & Forte, 2004) studied the relation between gravity field and land uplift rates in Fennoscandia and showed a significant correlation between them. Later, Svensson (1980) showed that the land uplift rate matches a viscosity of about 5×10^{22} Pa s in Fennoscandia. A similar study was performed by Simons and Hager (1997) and found a correlation between the gravity field and the land uplift rate in Hudson Bay. They also determined a viscosity model in Laurentia and Fennoscandia using land uplift rates and the GIA-related gravity field. They showed that a −31 m geoid depression that is related to the GIA in the Hudson Bay (cf. Joud, 2018; Sjöberg & Bagherbandi, 2017) presented the corresponding geoid height depression (due to GIA) in Fennoscandia varies between −8.9 and 0.19 m, with a mean value of -5.5 ± 2.1 m for the spectral window between degrees 10 and 23 (cf. Bjerhammar et al., 1980). They showed that the spectral window was most correlated with the land uplift rate and the geoid. However, we know that the geoid varies between 15 up to 45 m in Fennoscandia. Therefore, the GIA-related gravity signal is implicitly hidden in the Earth's gravity field (cf. Joud, 2018). In fact, the harmonic window between degrees 10 and 23 is related to the GIA and is corresponding to the maximum −8 m geoid height in the center of the uplift dome in Sweden. Therefore, the obtained GIA-related gravity signal can be used to determine the mantle viscosity using the land uplift rate and the truncated gravity field (cf. Bjerhammar et al., 1980; Sjöberg & Bagherbandi, 2013). However, Root et al. (2015) used a different harmonic window to determine the GIA-related gravity field that is, $4 \leq n \leq 45$. The major part of the long-wavelength gravity field signals ($n < 10$) is explained by mantle convection of subduction slabs (Mishra & Kumar, 2012; Richards et al., 1988). Therefore, the viscosity is better constrained for the upper (less than 670 km depth) than the lower mantle (Mitrovica & Peltier, 1991). Viscosity can also be determined by fitting predicted viscosity models to the GIA-related observations such as vertical land motions derived using GPS permanent stations. It is worth mentioning that these methods are dependent on the Earth's interior structure (i.e., rheology) and load history (W. R. Peltier, 1996).

Land uplift modeling plays an important role in the processes related to the Earth system. Studying the land uplift rate allows us to investigate the long-term development of the Earth's shape, interior and gravity field, which affects a vast number of other phenomena such as those related to the prediction of climate change and sea-level rise. GIA-related land uplift rate can be observed using different measurements such as relative sea-level rise, tide gauge, GNSS data, and gravity field changes observed at the Earth's surface by employing absolute gravimeters (Olsson et al., 2019). In addition, the land uplift can be obtained using satellite gravimetry techniques that is, the gravity recovery and climate experiment (GRACE) and GRACE Follow-on missions (Shafiei Joud et al., 2017). In Greenland, the land uplift has been determined using relative sea-level rise data obtained from tide gauges, GPS data (Khan et al., 2016), and absolute gravimeters. One of the important data for studying the temporal

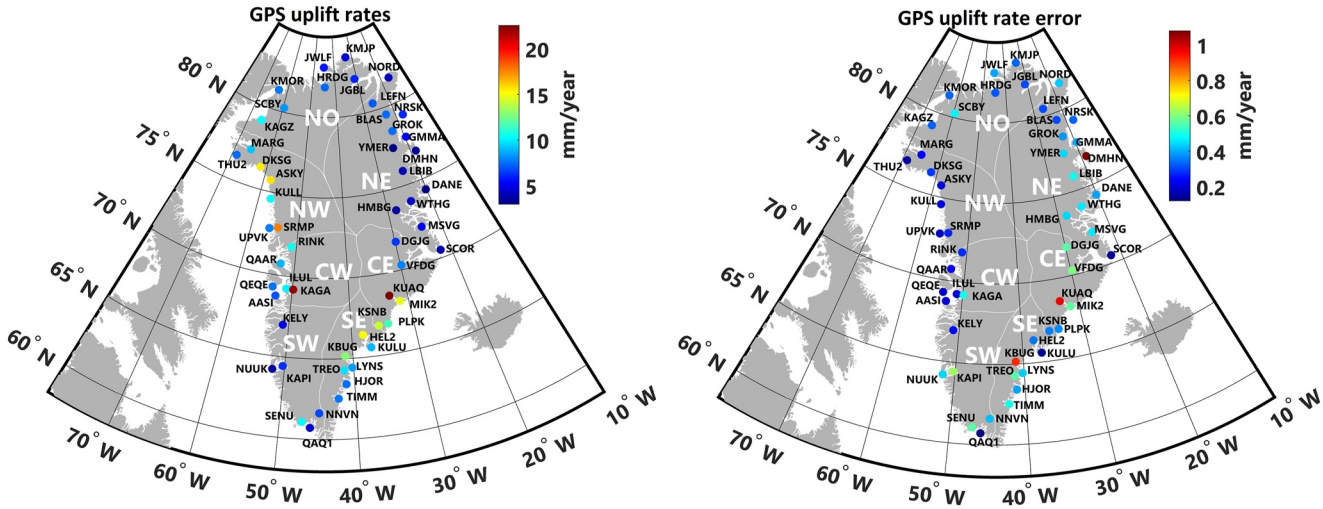

Figure 1. Vertical displacement rates (left) at the Greenland Global Positioning System (GPS) Network (GNET) sites and their uncertainties (right) according to Khan et al. (2016). Unit: mm/year.

changes of the gravity field obtains from the dedicated satellite gravity mission GRACE that will be used in this study. Many scholars have used the GRACE monthly data to study mantle rheology and ice history in areas with GIA and land uplift phenomena (e.g., Argus et al., 2021; Paulson et al., 2007; Zhao, 2013). The satellite-based data are from low-orbit dedicated missions with a homogeneous coverage. The satellite data suffers from inherent data processing problems (such as removing noises) and need to be adequately addressed to achieve reliable data with the desired accuracy. In addition, we will compare the discrepancy between the GRACE-based land uplift rates, the inferred vertical displacement rates at the GNET sites, and the GIA models like ICE-6G (VM5a) and Caron et al. (2018) models in Greenland. For this study, we will use the GRACE data from 2003 to 2016 as well.

In this paper, we study the upper mantle viscosity determination by inferring the gravity field signal related to the GIA in Greenland. For this purpose, we use the land uplift rate obtained from GNET (Khan et al., 2016), GIA models (ICE-6G (VM5a) model (Peltier et al., 2013; Caron et al., 2018)), and the GRACE data in Greenland. We know that the uncertainty is also significantly large in the glaciated regions (Ludwigsen et al., 2020). Therefore, we integrate these data because the uncertainties, patterns and rates of the land uplift models are different in Greenland. The applied method procedure (in this study) is as follows. In Step 1, we recover the GIA related GNSS uplift rates (determined by Khan et al. (2016)) and GRACE data. In addition, we present a combined land uplift rates using GNSS, GRACE and GIA-derived land uplift rates. In Step 2, we extract the GIA-related gravity signals by filtering the other effects due to the deeper masses that is, core-mantle (related to long-wavelengths) and topography (related to short-wavelengths). To do this, we applied correlation analysis for this purpose and to detect the best harmonic window over which modeled GIA most depends (not the window over which other phenomena like dynamic topography or surface topography). Finally (in Step 3), we estimate the mantle viscosity using the GIA-related gravity field according to the method developed by Bjerhammar et al. (1980) and Sjöberg and Bagherbandi (2017).

2. Data

2.1. GPS Data

We used the GPS-derived vertical displacement rates obtained from the Greenland Global Positioning System Network (GNET) in this study (see Figure 1), which were published by Khan et al. (2016). There are a total number of 53 GNET GPS sites. They directly measured the GIA and studied basin-wide mass changes since the last glacial maximum. The Earth's crust responds to the internal and external forces, and many short-term elastic readjustments are tangible due to the contemporary mass balance changes and tectonics. In other words, the elastic rebound is due to the short-wavelength components of the vertical uplift in response to the current ice mass loss (Spada et al., 2012). Therefore, the elasticity correction (present-day mass loads) is required to extract

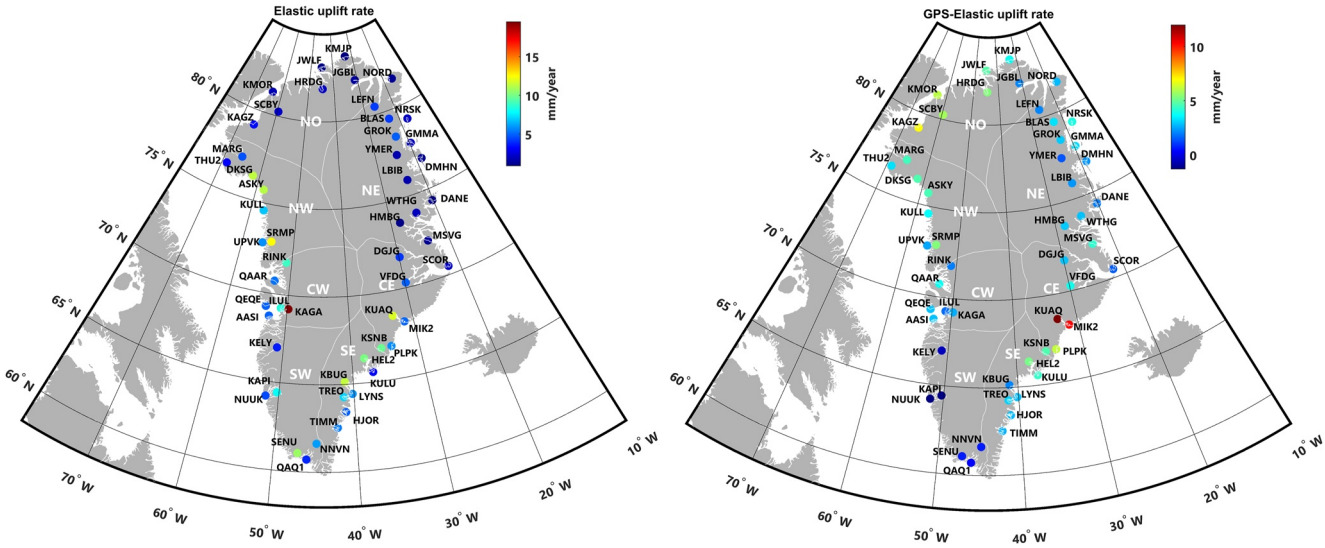

Figure 2. Elastic uplift rate correction (left, according to Khan et al. (2016)) and corrected vertical displacement rates (from GPS data) after adding the elastic correction (right). Unit: mm/year.

the GIA-related uplift rates. The impact of the elasticity should be removed from the observed GPS uplift rates because the ground surface responds to the GIA and contemporary ice sheet melting in Greenland. However, Khan et al. (2016) believe that the tectonic deformation can be considered negligible. In addition, they used satellite and airborne laser and satellite radar altimetry data to model the ice mass changes and then removed the elastic effect at each GNET site. Different datasets were used for modeling the elastic correction, such as NASA's Airborne Topographic Mapper (ATM) flights from 1995 to 2014, laser altimetry observations from the Ice, Cloud, and Land Elevation Satellite (ICESat) from 2003 to 2009, the airborne Land, Vegetation, and Ice Sensor (LVIS) observations from 2007 to 2013, radar altimetry data from the CryoSat-2 from 2010 to 2015, and the European Remote-Sensing Satellite–1 (ERS-1) and ERS-2 data during 1995–2003. The elastic correction can be obtained by converting the volume loss rate into a mass loss rate, as presented in Kuipers Munneke et al. (2015). Finally, the obtained mass loss changes were convolved using Green's function for determining the land uplift rates derived by Petrov and Boy (2004). Figure 2 shows the estimated elastic land uplift rates based on the load changes obtained from radar/laser altimetry observations and GPS uplift rates corrected by the elastic effect. The applied elastic correction was provided by Khan et al. (2016).

2.2. GIA Model

There are different GIA models on a global scale that can be used for estimating the viscosity parameter in this study. A review of the GIA models in Greenland can also be seen in Wake et al. (2016). The GIA models show significant discrepancies in Greenland, which can be seen from the GIA model patterns and rates. For example, Figure 3 shows the GIA uplift rates (land uplift) obtained from two GIA models: ICE-6G (VM5a) (Peltier et al., 2013) and the model presented by Caron et al. (2018). The differences reflect the uncertainties about the glacial history (melting since the Last Glacial Maximum) and solid Earth rheology according to Kappelsberger et al. (2021). Generally, GIA models use a global ice and Earth model as input data. One of the purposes of this study is to combine different GIA-related uplift rates using the Kalman filtering method to obtain a better GIA uplift rate model. To do this, we need the uncertainty of the GIA model (Caron et al., 2018). GIA model provides this information for our purpose that will be used in this study. Figure S1 in Supporting Information S1 shows the uncertainty of the GIA uplift rates in the GNET sites.

2.3. GRACE Data

The Gravity Recovery and Climate Experiment (GRACE) mission, with more than 19 years of observations can be used to model the Earth's mass redistribution within the Earth system and ice sheet melting at large

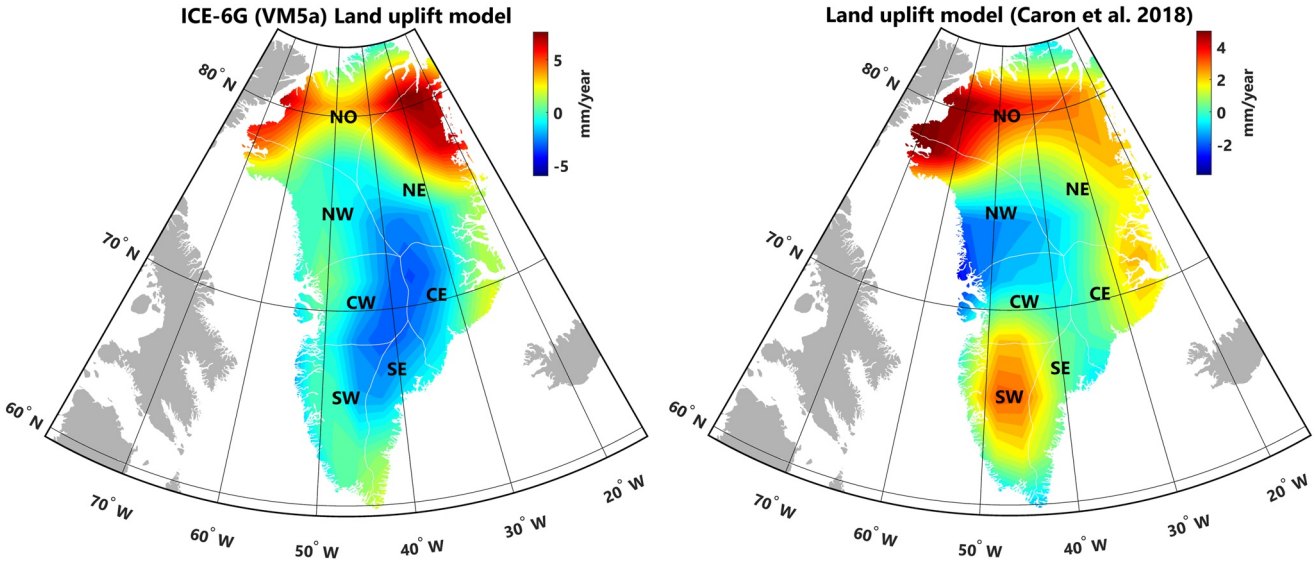

Figure 3. GIA-related uplift rates obtained from ICE-6G (VM5a) model (left) presented by Peltier et al. (2013) and Caron et al. (2018) GIA model (right) in Greenland. Unit: mm/year.

scales (Tapley et al., 2004). Here we employed the level 2 monthly spherical harmonic coefficients of GRACE Release 05 provided by the Center for Space Research (CSR) at the University of Texas with a truncation of up to degree 60 (the data are available via http://icgem.gfz-potsdam.de/home). The GRACE data is used for estimating vertical displacements in Greenland. The relationship between the vertical component (land uplift rate) and the Stokes mass coefficients was studied by Kusche and Schrama (2005), van Dam et al. (2007), and Sjöberg and Bagherbandi (2017). More details can be seen in Section 3.1.

3. Methodology

3.1. Determination of Land Uplift Rate Using GRACE Data

The land uplift in the areas with GIA phenomena implies that the deloading of the previous ice sheet results in a continuous rising of the depressed crust. The deviation of the gravity field from the isostatic balance can be formulated in terms of the remaining depressions of the Earth's crust and the geoid. To determine the land uplift rate using the GRACE monthly data, we suppose that the Earth's crust different layers are equally deformed because of the ice load. According to Sjöberg and Bagherbandi (2013) and Sjöberg and Bagherbandi (2017), the crust depression due to a continental glacier will affect the disturbing potential in upper and lower layers at sea level, and it is expressed by:

$$\begin{aligned}\Delta T &= T_{\mathrm{GIA}}^{\text{upper layer}} - T_{\mathrm{GIA}}^{\text{lower layer}} \\ &= -G\rho_c \iint_{\sigma} \int_{R-d}^{R} \frac{r^2 dr}{l} d\sigma - G\Delta\rho \iint_{\sigma} \int_{R-D-d}^{R-D} \frac{r^2 dr}{l} d\sigma\end{aligned} \tag{1}$$

where $T_{\mathrm{GIA}}^{\text{upper layer}}$ is the effect of the mass deficit on the disturbing potential and $T_{\mathrm{GIA}}^{\text{lower layer}}$ shows the effect of mass deficit due to the depressed lower crust into the mantle. G is the gravitational constant, ρ_c is the crust density, $\Delta\rho$ is the crust-mantle density contrast, R is the Earth mean radius, l is the distance between the computational point and integration point, D is the crust thickness or Moho depth (cf. Bagherbandi et al., 2013), and d donates on the crust depression. By employing the exterior type of the Legendre series and the first-order Taylor series approximations, Equation 1 can be written in the spectral form:

$$\Delta T = -4\pi G\rho_m R \sum_{n=0}^{\infty} \frac{1}{2n+1} \sum_{m=-n}^{n} d_{nm} Y_{nm}, \tag{2}$$

where ρ_m is the density of the upper mantle. We rewrite Equation 2 by assuming that the land uplift (h) is the opposite of the glacial depression process that is, $d = -h$ (Sjöberg & Bagherbandi, 2013):

$$\dot{h} \approx \frac{1}{4\pi G\rho_m R}\sum_{n=0}^{\infty}(2n+1)\dot{T}_n \tag{3}$$

where $\dot{T}$ denotes on the secular rate of ΔT for example, obtained from the GRACE monthly data and $\dot{h}$ is the land uplift rate.

The changes in the gravity field ($\dot{T}$) is determined using the time series analysis explained in Sjöberg and Bagherbandi (2017) and Wang et al. (2019). The GRACE Stokes coefficients and load Love numbers can be used to estimate the surface displacements induced by the surface mass loading, according to the elastic loading theory (Farrell, 1972). In this study, the gridded mass estimates from GRACE were convolved with the Green's function computed according to Jentzsch (1997) for PREM (Dziewonski & Anderson, 1981) to predict surface displacements. Here, a gridded scaling factor is generated to restore the GRACE predictions of the crustal displacements from CSR Release 5 (RL05) spherical harmonic coefficients (up to maximum degree 60) using forward modeling and surface mass fields. The unscaled land uplift rates calculated from GRACE multiplied by the scaling factors was used to estimate the downscaled GRACE prediction of the uplift in Greenland at 0.5-degree scale and in the GNET GPS sites. In the above, a summary of using GRACE data to estimate the land uplift rate was presented. For more details about the detailed formula, see Wang et al. (2019) and also Zhang et al. (2021).

3.2. A Combined Land Uplift Rate Using Kalman Filtering in the GNET Sites

Three datasets are combined in this study that is, the GIA up rates obtained from the GIA models, GNET sites and GRACE data. These data can be used as observations (inputs) in a Kalman filtering approach. The Kalman filtering is a well-known and iterative mathematical method that utilizes a set of equations and consecutive data (as initial and inputs data) to estimate the true value of a parameter being observed when the observations contain unpredicted or random error, uncertainty or variation. Simply, the Kalman filtering approach does not require a whole bunch of inputs, and it starts by taking an initial estimate and quickly starts to narrow into the true value by taking a few of those inputs. Kalman filtering uses three main equations iteratively that is, Kalman gain ($\boldsymbol{G}$) or weight, current estimate and its error. The Kalman gain shows how much we can trust the estimate and the measurements:

$$\boldsymbol{G} = \frac{\boldsymbol{e}_{\text{est}}}{\boldsymbol{e}_{\text{est}} + \boldsymbol{e}_{\text{mea}}}, \tag{4a}$$

We assume that the design matrix is an identity matrix (i.e., $\boldsymbol{A} = \boldsymbol{I}$) in the linearized observation equation that is, $\boldsymbol{L} = \mathbf{AX}$. Therefore, the measurements/observations vector ($\boldsymbol{L}$) will be equal to $\boldsymbol{X}$ (unknown parameters). Hence, the current estimate (updating estimate each time) is given by:

$$\boldsymbol{x}_t = \boldsymbol{x}_{t-1} + \boldsymbol{G}\left[\boldsymbol{L} - \boldsymbol{x}_{t-1}\right], \tag{4b}$$

Finally, the new error in the estimate can be calculated by:

$$\boldsymbol{e}_{\text{est}_t} = \frac{\boldsymbol{e}_{\text{mea}}\boldsymbol{e}_{\text{est}_{t-1}}}{\boldsymbol{e}_{\text{mea}} + \boldsymbol{e}_{\text{est}_{t-1}}} = [1 - \boldsymbol{G}]\boldsymbol{e}_{\text{est}_{t-1}} \tag{4c}$$

where $\boldsymbol{G}$ is Kalman gain, $\boldsymbol{e}_{\text{est}}$ is error in the estimate, $\boldsymbol{e}_{\text{mea}}$ is error in measurements or observation, $\boldsymbol{x}_t$ and $\boldsymbol{x}_{t-1}$ are current and previous estimates, respectively.

The current estimate is obtained using the previous estimate plus the difference between the measured value and the previous estimate controlled by Kalman gain as a weight. Equation 4c is used to recalculate the error in the current estimate. If the error in the measurement is very large, the error in the estimate will not change very quickly and vice versa.

3.3. Upper Mantle Viscosity Determination Using a Gravimetric Approach

We follow Sjöberg and Bagherbandi (2013) to determine the mantle viscosity. They presented an inverse solution to this gravimetric boundary value problem in terms of the remaining depression of the load of the ice mass (see also Sjöberg and Bagherbandi (2017)). The employed approach considers the Earth as a viscoelastic body for determining the upper mantle viscosity. The approach is based on an a-priori assumption of linear rheology of the upper mantle. The method needs two data sets: GIA-related gravity field and land uplift rate. The geopotential magnitude and pattern should reflect the ongoing rebound. The relation between decay time (i.e., the amount of time it takes for the remaining equilibrium to be reduced due to the ice load) and the remaining land uplift can be written using the following exponential function (cf. De Geer, 1888; Niskanen, 1949; Walcott, 1980):

$$h_n = (h_0)_n \, e^{-t/\tau_n} \tag{5a}$$

where t is time, h_0 denotes the total depression at time $t = 0$, τ_n is the spectral decay and $e \approx 2.67$ is the base of the natural logarithm. It is worth mentioning that relaxation time has an inverse relation with the decay time. By differentiating Equation 5a with respect to time:

$$\dot{h}_{\mathrm{n}} = d_{\mathrm{n}}/\tau_{\mathrm{n}} \tag{5b}$$

After inserting Equation 5b into Equation 3, the decay time can be written:

$$\tau_{\mathrm{n}} \approx -\frac{1}{4\pi G \rho_{\mathrm{m}} R} \sum_{\mathrm{n}=0}^{\infty} (2\mathrm{n}+1) \frac{T_{\mathrm{n}}}{\dot{h}_{\mathrm{n}}} \tag{6}$$

According to W. R Peltier (1974) and Mitrovica and Forte (2004) the decay time is only dependent on viscosity and density. Therefore, the decay time can be converted to viscosity (cf. Cathles III, 1975; Sjöberg & Bagherbandi, 2013):

$$\tau_{\mathrm{n}} = -\frac{\eta_{\mathrm{n}}}{\gamma \rho_m R} \left(2\mathrm{n} + 4 + \frac{3}{\mathrm{n}}\right) \tag{7}$$

Inserting Equation 6 in Equation 7, the viscosity of mantle will be obtained:

$$\eta \approx -\frac{\gamma}{4\pi G} \sum_{n=0}^{\infty} \frac{2\mathrm{n}+1}{2\mathrm{n}+4+3/\mathrm{n}} \frac{T_{\mathrm{n}}}{\dot{h}_{\mathrm{n}}} \tag{8}$$

The relation between disturbing potential T and geoid height is defined by Bruns' formula (Heiskanen & Moritz, 1967). Finally, we infer the viscosity of the upper mantle from the geoid anomaly and land uplift rate using Equation 8. The correlation analysis between the geoid and a land uplift model is used to obtain the geoid anomaly (representing the remaining uplift to isostatic equilibrium). Figure 4 shows the employed method to estimate the viscosity using the geoid anomaly, which correlates with the land uplift rates. The land uplift rates can be obtained using the GIA models, the vertical land motion (related to GIA uplift rate) obtained by GNSS (i.e., GNET) and GRACE data or a combination of the above-mentioned land uplift rates (see Section 3.2). In other words, a combined land uplift model can be used if different available land uplift models are not statistically consistent. Here one can use hypothesis testing (see Appendix A) to evaluate the consistency of the land uplift models. If the test is passed, then every individual land uplift model can represent the data for the viscosity determination. Otherwise, the use of combined model is suggested.

4. Results and Discussions

This section presents the estimated mantle viscosities using five scenarios (two regional GIA models and three pointwise datasets in the GNET sites). We used different GIA-related land uplift models to determine the viscosity using Equation 8 such as ICE-6G (VM5a), the GIA model presented by Caron et al. (2018), GNET uplift rates (Khan et al., 2016), GIA-related uplift rates obtained from GRACE data, and the combined GIA-related vertical land motions obtained from Kalman filtering approach in Greenland. The EGM2008 model has been used to determine the geoid in all the above-mentioned scenarios.

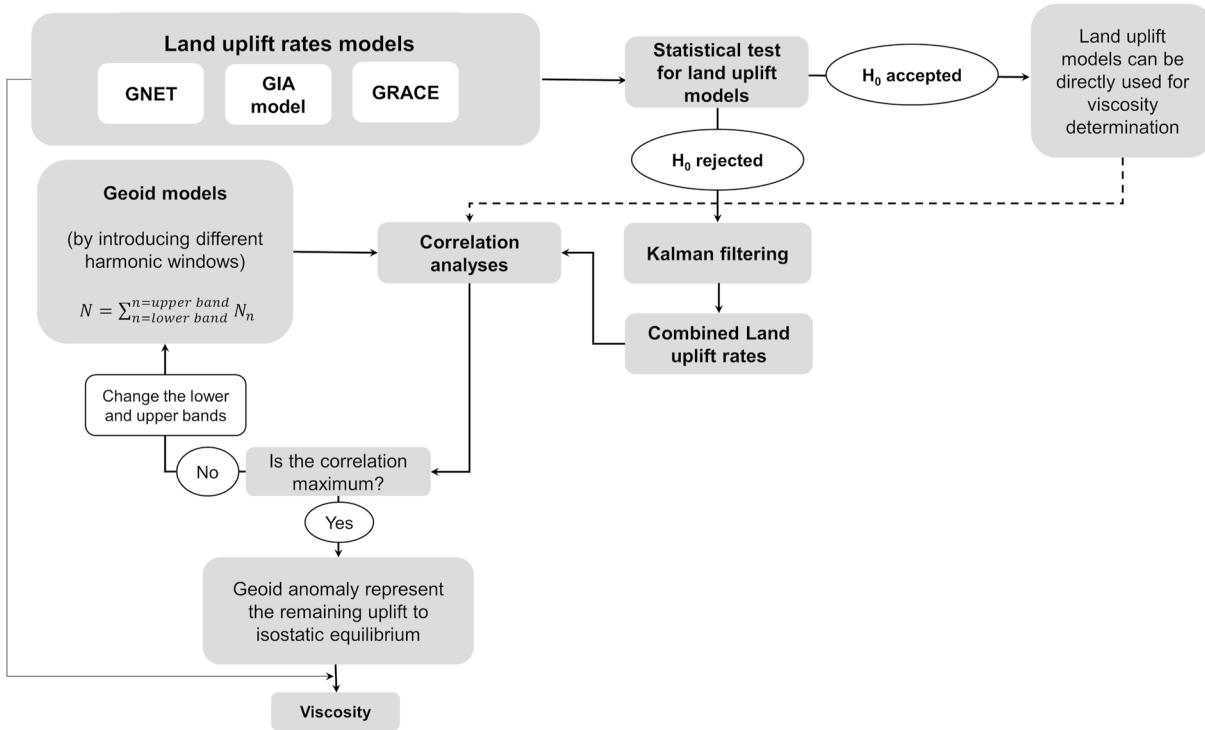

Figure 4. Flowchart of viscosity determination using geoid anomaly and different land uplift rates.

4.1. GRACE-Derived Land Uplift Rates

In this paper, we followed and used the technique presented by Wang et al. (2019) to model the vertical land motion in Greenland with a higher resolution than the spatial resolution of the GRACE data that is, 0.5° × 0.5° scale. As we mentioned in Section 3.1, Wang et al. (2019) used a down-scaling approach to enhance the mass change derived from the GRACE data by employing surface mass balance and observed surface elevation change in Greenland. The GNET data was used to evaluate the scaled GRACE-derived vertical displacements predictions. Moreover, the GRACE-derived vertical land motion predictions belong to the crustal response to the present-day mass changes in Greenland. Therefore, the elasticity correction should be applied to the GRACE-derived vertical land motion to determine the GIA-related uplift rates (similar to Section 2.1). Figure 5 shows the GRACE-derived uplift rates after applying the elastic correction in GNET sites. The GRACE-derived uplift rates (before applying the elastic correction) and their corresponding uncertainties are shown in Figure S2 in Supporting Information S1. In addition, the uncertainties of the GIA-related uplift rates after adding elastic correction using GNET and GRACE data were determined by the following equations:

$$\sigma_1^{\mathrm{GIA}} = \sqrt{\sigma_{\mathrm{GPS}}^2 + \sigma_{\mathrm{Elastic}}^2} \tag{9}$$

$$\sigma_2^{\mathrm{GIA}} = \sqrt{\sigma_{\mathrm{GRACE}}^2 + \sigma_{\mathrm{Elastic}}^2} \tag{10}$$

where σ_1^{GIA} and σ_2^{GIA} are the uncertainties of the GIA-related uplift rates, σ_{GPS} and σ_{GRACE} show the uncertainties of the uplift rates derived by GPS and GRACE data, respectively. $\sigma_{\mathrm{Elastic}}$ is the uncertainty of the elastic uplift rate correction that can be obtained from Khan et al. (2016). The results of $\sigma_1{}^{\mathrm{GIA}}$ and $\sigma_2{}^{\mathrm{GIA}}$ are illustrated in Figure S3 in Supporting Information S1. $\sigma_1{}^{\mathrm{GIA}}$ and $\sigma_2{}^{\mathrm{GIA}}$ will be used for combining the land uplift rate utilizing the Kalman filtering method (see Section 4.3).

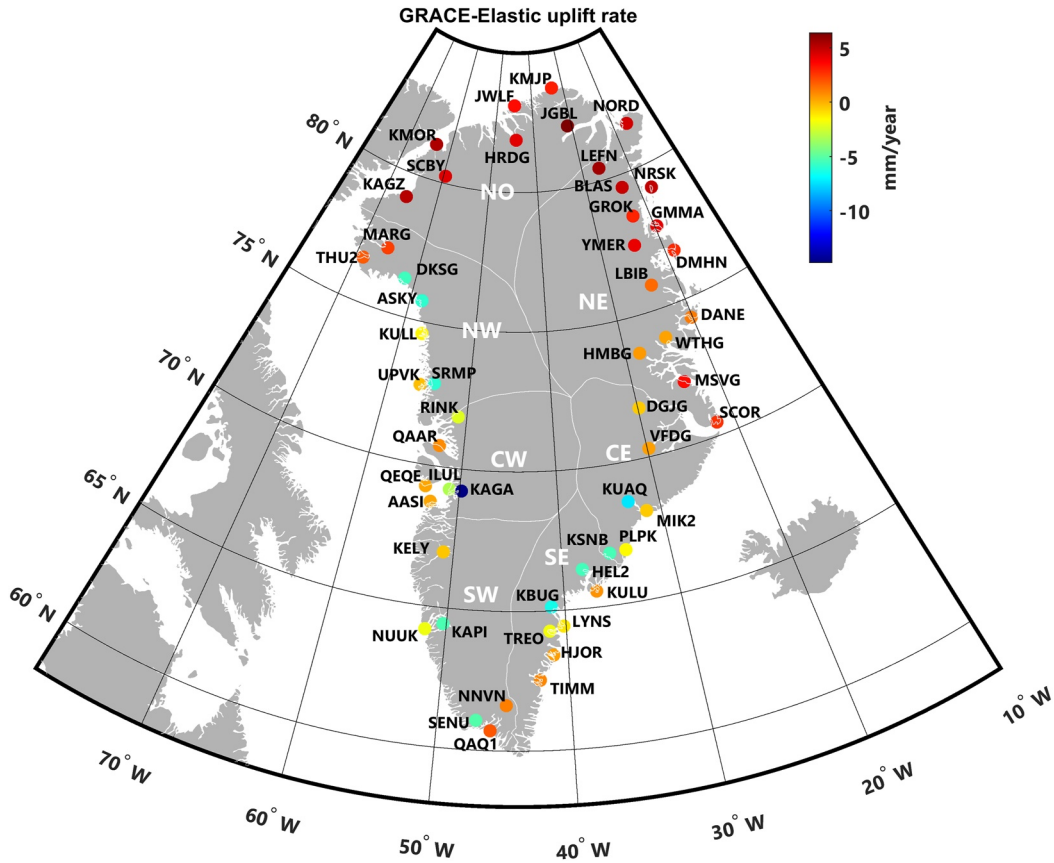

Figure 5. GRACE-derived recovery and climate experiment -derived vertical displacements after considering the elastic uplift rate correction in the Greenland Global Positioning System Network sites. Unit: mm/year.

4.2. Comparison of VLMs in GNET Sites

The uncertainty of the GIA models and the observations used for estimating the VLM (like GPS) can affect the lithosphere thickness and mantle viscosity determination (cf. Zhao et al., 2012). Therefore, the effect of the different VLM models for determining the viscosity should be assessed in advance. Table 1 shows the differences between the VLMs that have been used in this study. The observed GPS land uplift rates (without elastic corrections) show extreme VLM in some GNET sites for example, in KUAQ and KAGA stations in southeast and southwest Greenland. Khan et al. (2016) mentioned that an asthenospheric layer with low viscosity and likely existing the past hot spot track can impact ice sheet or glacier flow dynamics. Accordingly, the geothermal heat flux at the base of an ice mass will influence the internal thermal regime (see also Rogozhina et al. (2016)). These extreme values reconcile after considering elastic corrections. However, the land uplift rate models show different magnitudes and patterns in Greenland (see e.g., Figure 3). This is the main reason to combine different land uplift rates to reduce the remaining errors/uncertainties in this study. However, it will be reasonable to test different uplift rates statistically first. This evaluation can be performed by employing null (H_0) and alternative (H_a) hypotheses for example, by assuming $\alpha = 5\%$ significance level, as presented in the Appendix A. Using the hypothesis test, one can evaluate whether the vertical land motions (VLM) obtained from GRACE, GPS and GIA models belong to the same population and are similar or not. The results of the statistical hypothesis testing have been shown in Figure S4 in Supporting Information S1. The obtained VLMs from the GIA model, presented by Caron et al. (2018), are more consistent with the VLM derived from GRACE and GPS data. Although, the outcomes illustrate that the obtained VLMs are not similar in some of the GNET sites.

Table 1
Statistics of Differences Between Different VLMs Were Applied in This Study

	GPS-GRACE	GIA-GRACE	GIA-GPS
Max	18.2	7.9	3.5
Min	−2.8	−6.7	−17.2
Mean	3.2	−1.0	−4.2
Std	4.6	3.1	4.8

Note. Unit: mm/year.

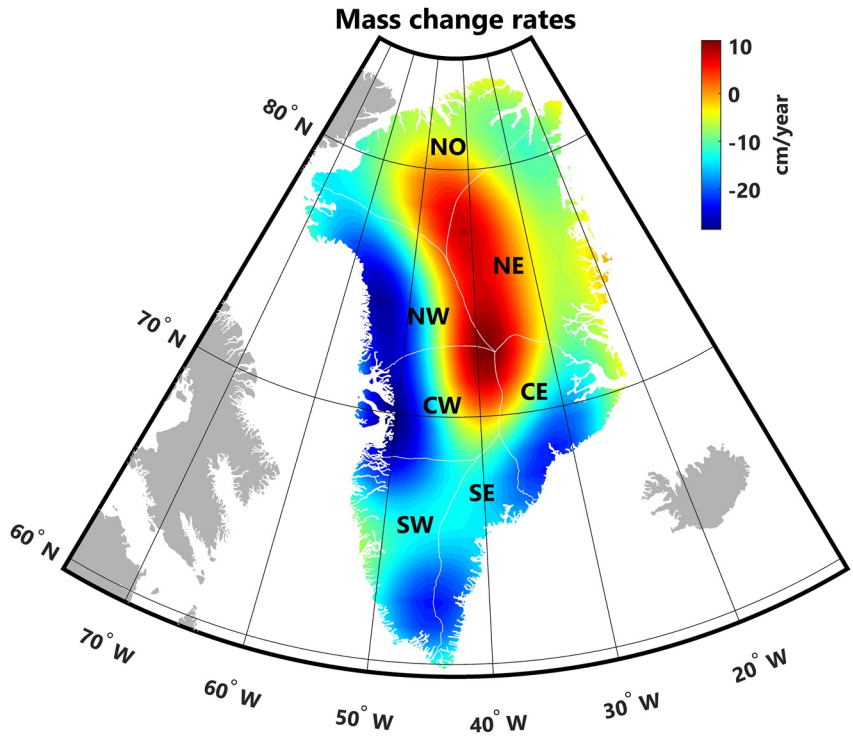

Figure 6. Surface mass change rates in terms of equivalent water height change over 2003–2016 in Greenland. Unit: cm/year.

The results of the statistical hypothesis testing illustrate that 14 and 17 stations are rejected when one compares the GRACE- and GPS-derived VLMs, respectively, with the GIA model. The consistency of the GRACE- and GPS-derived VLMs is not high because of the 46 rejection rate. The number of rejections also depends on the uncertainties of GRACE and GPS data. The extreme discrepancies between the GPS- and GRACE-derived VLMs are observed in the southeast and western part of Greenland, where the stations are experiencing a decreasing mass loss with time (i.e., in NW, CW, CE, SE, and SW major regions of the Greenland ice sheet). The discrepancies can result in more considerable uncertainty in estimating the viscosity due to the uncertainty of the elastic model. Therefore, a combined land uplift model conceivably compensates for the discrepancies and will be helpful for our purpose. In other words, since the obtained land uplift from GNET, GIA and GRACE models are not statistically similar (see Figure 4), a combined model using Kalman filtering is suggested (see Section 4.3). It is worth mentioning that all stations (even rejected ones) are used to combine the land uplift rates derived from GIA, GRACE and GPS data in this study.

Solid Earth is not only deforming in viscous response to the last ice age today, but it is also responding elastically to the recent surface mass changes, including ice melting over Greenland. For instance, Northern Canada has risen 0.5–3 mm yr^{-1} over the past 25 years in an elastic response to the present-day ice melting over Greenland, the Canadian Arctic Archipelago, and southeast Alaska (Argus et al., 2021). Figure 6 shows the regional distribution of the surface mass change rates in terms of equivalent water height change using GRACE RL06 data over 2003–2016 in Greenland (see more theoretical details in Wahr et al. (1998) and Amin et al. (2020)). As can be seen, the west side of Greenland is losing the most ice mass, following by center-east (CE) and south-east (SE) regions. One can see that the highest uplift rates are related to the stations located in regions with the highest rate of ice melting (see Figure 1). This correlation indicates an obvious elastic response of the solid Earth to the modern short-period ice mass loss in Greenland. Accordingly, the elastic correction should be applied to the GPS-based uplift rates. However, the uncertainty of the elastic correction can be one of the reasons for the discrepancy between the GIA model and other land uplift models obtained by the GPS and GRACE data.

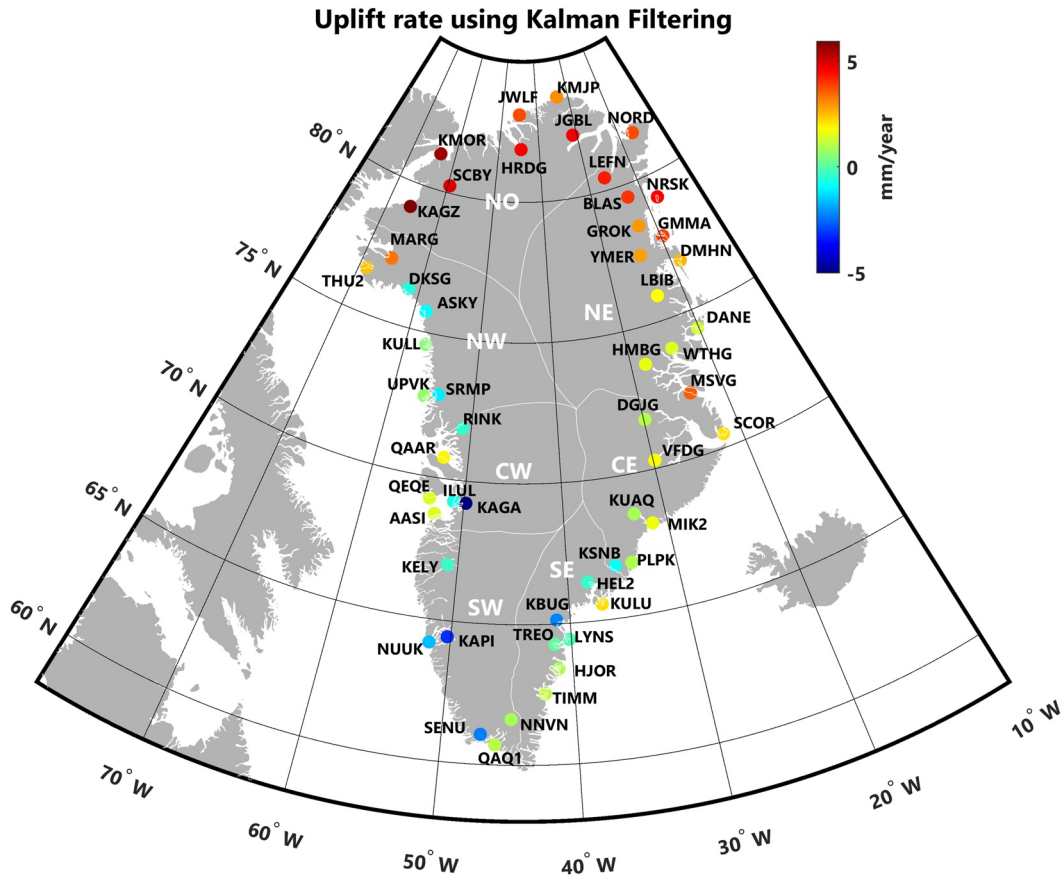

Figure 7. Estimated uplift rates at the Greenland Global Positioning System Network sites using the Kalman filtering approach. Unit: mm/year.

4.3. Combined GIA-Related Land Uplift Rate Obtained Using Kalman Filtering Approach

We utilize the described Kalman filtering approach (Section 3.2) to combine different land uplift rates in this study. We assume that the land uplift rates obtained from Caron et al. (2018) GIA model as an initial value and the uplift rates obtained from the GNET and GRACE data as measurements. The combined uplift rate obtained from the Kalman filtering approach in the GNET sites can be seen in Figure 7. A comparison of the Kalman filtering results and the uplift rates obtained from GRACE, GPS and the GIA model can be seen in Figure S5 in Supporting Information S1. Figure S5 in Supporting Information S1 shows that the forward and backward Kalman filtering methods provide the same results because the uncertainties of the initial values are low. The uncertainty of the estimated uplift rates is presented in Figure S6 in Supporting Information S1. Using the Kalman filtering approach, the obtained uplift rate error varies 0.48 to 0.07 mm/year with a mean value of 0.20 and a standard deviation of 0.10 mm/year. As we mentioned before, large errors can be observed in the stations experiencing extreme decreasing ice mass loss (e.g., SRMP, RINK, KAGA, KBUG, HEL2, and KUAQ stations).

It is worth mentioning that we presented only the Kalman filtering results in this study. Different techniques can be used to combine the GPS, GRACE and GIA-derived land uplift rates such as simple least squares adjustment, an enhanced least squares method by estimating variance component estimation (VCE) technique (cf. Amiri-Simkooei, 2007; Helmert, 1924; Rao, 1971; Sjöberg, 1983), and Kalman filtering. There is no doubt that the post-glacial rebound is a dynamic (time-variable) process. Usually, the Kalman filter is used in recursive processes, but it could also be implemented in batch processes. However, when dealing with a dynamic phenomenon, incorporating the dynamic model into the least squares' solution (which is the Kalman filter in the batch process) gives us extra information that leads to better estimates. In addition, the redundancy and degree of freedom (df = 2) are low in this study. Therefore, if one uses simple least squares adjustment, the estimated unknown

parameter's quality (land uplift rate in each station) will not be good. A higher degree of freedom provides more power to reject a false null hypothesis and find a significant result.

4.4. Harmonic Window Analysis and Viscosity Determination

The viscosity of the upper mantle can be determined using Equation 8. However, first, the geoid anomaly (that represents the remaining uplift to isostatic equilibrium) should be determined by correlation analysis between the geoid and land uplift rate. The correlation analysis will reveal the harmonic window of the geoid that can sense the present glacial-isostatic relaxation of the Earth's lithosphere. The obtained harmonic window will also show the depth of the gravity signal (i.e., the values to a specific depth interval in the mantle), for example, using Bowin (2000) definition for the ratio of gravity to geoid anomalies as a function of depth to a point-mass source. Figure 8 shows the results of correlation analysis to find the best geoid signal harmonic window. We utilized the Pearson method to find the correlation between the land uplift models in Matlab software. To perform this, we change the spherical harmonic windows from the lowest degree (i.e., $n = 2$) to higher degrees to find the harmonic window that represents the remaining uplift to isostatic equilibrium. In other words, we seek the lower and upper harmonic bands in this step (see also Figure 4). We employed different land uplift rates, as mentioned already, to find the maximum correlation between the geoid signal and the land uplift rates (in a certain harmonic window). Figures 8a and 8b illustrate the correlation coefficients derived by harmonic window analysis between the geoid and land uplift rates from ICE-6G (VM5a) and (Caron et al., 2018) GIA models. The figures show that the most suitable harmonic windows are $10 \le n \le 39$ and $11 \le n \le 26$ using ICE-6G (VM5a) and (Caron et al., 2018) GIA models, respectively, because of the highest correlation coefficients between the obtained lower and upper bands. Similar plots can be obtained for the uplift rates in GNET sites (Khan et al., 2016), GIA-related uplift rates obtained from GRACE data, and the combined GIA-related vertical land motions in Greenland obtained using Kalman filtering.

Table 2 shows the mean value of mantle viscosities associated with different harmonic windows and different land uplift models, called Scenario 1–5 in the table, using Equation 8. The viscosities vary between 1.3×10^{21} and 1.9×10^{22} Pa s depending on the land uplift model used for viscosity determination. It is worth mentioning that the negative viscosity values, obtained in some stations, were removed from the calculations. It also shows the harmonic window and maximum correlation between the geoid signals and the utilized land uplift models. We observe lower correlation coefficients compared to other regions between the geoid and land uplift rates for example, Laurentia and Fennoscandia (cf. Bjerhammar et al., 1980; Sjöberg & Bagherbandi, 2013). One reason can be (probably) experiencing a decreasing mass loss with time in Greenland and the employed elastic correction for the land uplift models obtained from GPS, GRACE and combined model. One can observe that other upper bands could also be used as a harmonic window (in Figure 8). For example, Figure 8a shows the highest correlation considering a lower band equal to $n = 10$ and a higher band between $n = 39$–48. However, we used $n = 39$ because higher harmonics (i.e., $10 \le n \le 48$) provided a similar result. The estimated viscosity utilizing $10 \le n \le 48$ is equal to 1.4×10^{22} versus 1.9×10^{22} Pa s when one uses $10 \le n \le 39$. Therefore, the lower band on the harmonic window from the fact that the assumed exponential viscous decay rate breaks down as buoyancy from the core-mantle boundary becomes significant (see Cathles III (1975)). Hence, the selection of harmonic windows with slightly smaller correlations generates useable uncertainties for the viscosity.

In addition, the uncertainty of the obtained viscosities can be calculated using the propagation of uncertainty method. To calculate the uncertainty of the viscosity, one can simplify Equation 8 to the following form (cf. Sjöberg and Bagherbandi (2017)):

$$\eta \approx -\frac{\gamma}{4\pi G}\frac{T}{\dot{h}} \tag{11a}$$

Because it can be considered that the GIA is a regional phenomenon and mainly related to harmonics of degrees (e.g., larger than a harmonic of degree 10). Therefore, the ratio $(2n + 1)/(2n + 4 + 3/n)$ in Equation 8 is nearly to one for all degrees larger than 10, which yields Equation 11a. The uncertainties in the obtained viscosities ($u(\eta)$) can be obtained using the propagation of uncertainty method:

$$u(\eta) \approx \pm\frac{\gamma}{4\pi G}\sqrt{\left(\frac{1}{\dot{h}}\right)^2 u^2(T) + \left(-\frac{T}{\dot{h}^2}\right)^2 u^2\left(\dot{h}\right)} \tag{11b}$$

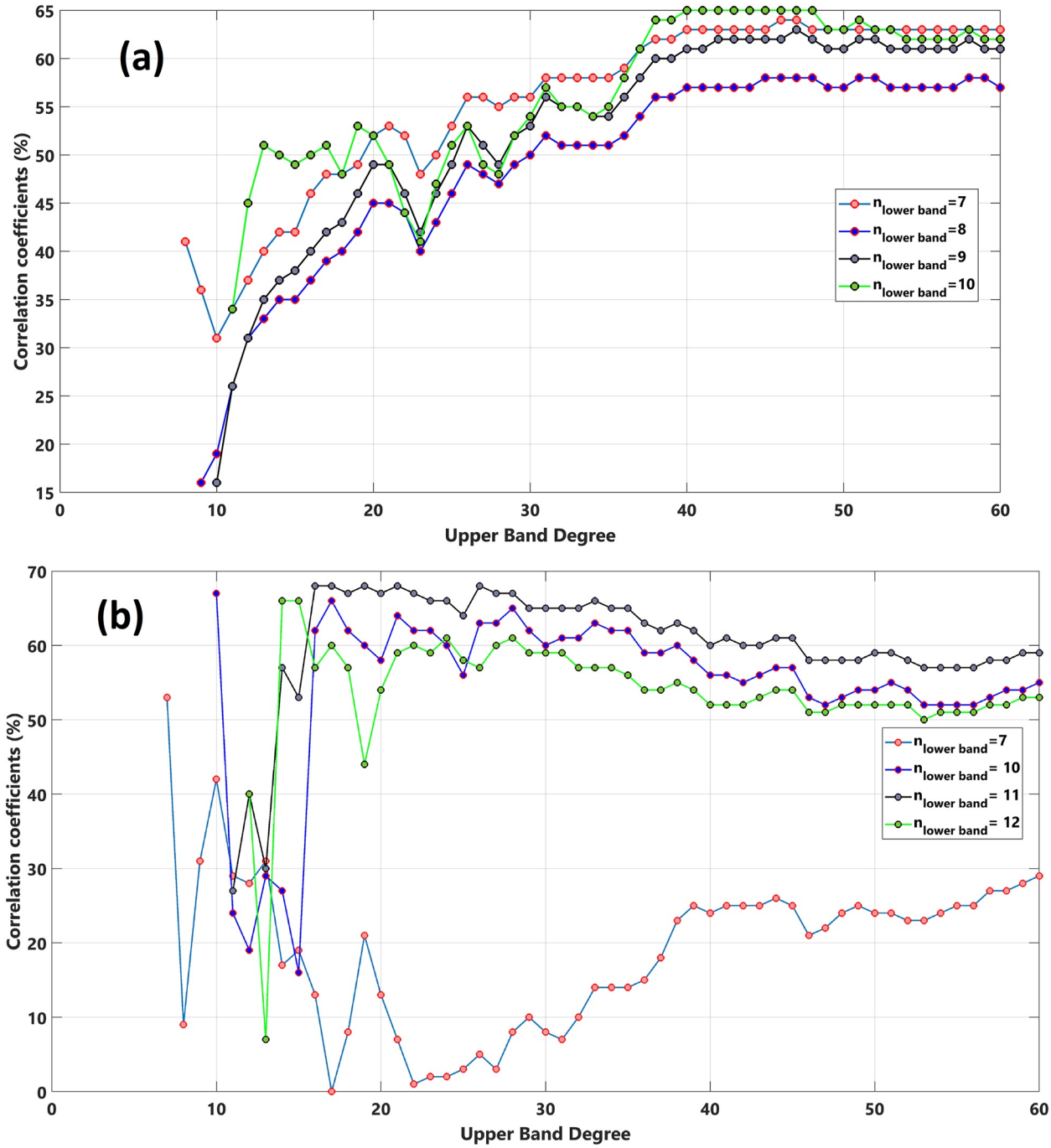

Figure 8. Correlation coefficients derived by harmonic window analysis between the geoid and vertical land motion obtained using (a) ICE-6G (VM5a) and (b) Caron et al. (2018) models.

where $u(T)$ and $u(\dot{h})$ are the uncertainties of the disturbing potential and land uplift rates. The obtained uncertainties can be seen in the last column of Table 2.

The truncated geoid models, using presented harmonic windows in the table, are related to different depths of the causative masses according to Figure 9, modified after Bowin (2000). Hence, the estimated viscosities are related to different radial boundaries in the mantle. For example, the estimated viscosities (see Table 2) can be related to the depth interval of the viscosity layer between 200 and 700 km (except Scenario 3 that can be related to layers between 200 and 400 km).

Table 2
Mantle Viscosity Obtained Using Different Scenarios in This Study

Scenarios	Data	Harmonic window	Correlation coefficient	Viscosity (unit: Pa s)	Uncertainty (unit: Pa s)
Scenario 1	EGM2008 & ICE-6G (VM5a)	$10 \leq n \leq 39$	0.65	1.9×10^{22}	–
Scenario 2	EGM2008 & Caron et al. (2018)	$11 \leq n \leq 26$	0.68	9.2×10^{21}	1.2×10^{17}
Scenario 3	EGM2008 & GNET uplift rate	$18 \leq n \leq 25$	0.40	1.3×10^{21}	2.6×10^{16}
Scenario 4	EGM2008 & GRACE GIA uplift rate	$11 \leq n \leq 26$	0.68	5.1×10^{21}	1.2×10^{17}
Scenario 5	EGM2008 & Combined GIA uplift rate	$11 \leq n \leq 26$	0.68	7.8×10^{21}	1.4×10^{17}

It should be mentioned that our results using for example, Scenarios 1, 2, 4 and 5 are over an order (or half) of magnitude greater than the estimates in the literature. The obtained results in this study are comparable with the other studies performed by other scholars. For instance, Lambeck et al. (2017) independently analyzed the relative sea-level change and tilting of palaeo-lake shorelines and, accordingly, developed a GIA model for North America and estimated mantle viscosity for the upper mantle to be 0.51×10^{21} Pa s. However, they estimated the viscosity of the lower mantle to be 13×10^{21} Pa s. In the VM5a model (W. R. Peltier et al., 2015), the viscosity of the upper mantle is constrained to be about 0.5×10^{21} Pa s based on the Fennoscandia relaxation spectrum. However, in the VM5a model, the viscosity of the top 600 km of the lower mantle (670–1,260 km depth) is estimated to be 1.57×10^{21} Pa s. Roy and Peltier (2017) presented a detailed comparison of the viscosity variations with depth between VM5a, VM6, and VM7 viscosity profiles. They showed radial viscosity structure of the VM5a, VM6 and VM7 viscosity profiles down to the core–mantle boundary (see Table 2 in Roy and Peltier (2017)). For example, they presented the mantle viscosity (for 420–670 km depth) using VM5a, VM6, and VM7 models are consistent and varies between 0.45 and 0.5×10^{21} Pa s. Lau et al. (2016) reported the mean upper mantle viscosity to be 0.3×10^{21} Pa s, the average viscosity of the top 1,500 km of the mantle to be 1.0×10^{21} Pa s, and the average viscosity of the lower mantle to be 5.0×10^{21} Pa s. In their viscosity profile, the viscosity of the top of the lower mantle is 1.3×10^{21} Pa s. Paulson et al. (2007) analyzed the relative sea-level changes along the east coast of North America and GRACE observations of the Earth's gravity changes and estimated the viscosity of the top of the lower mantle to be 2.3×10^{21} Pa s. Caron et al. (2018) used the relative sea-level change and GPS vertical rate datasets and aimed to estimate uncertainties in predictions of the GIA models by varying the ice history and mantle viscosity profiles. Accordingly, they reported 0.6×10^{21} Pa s for the upper mantle viscosity and 2.3×10^{22} Pa s for the lower mantle viscosity. Zhao (2013) analyzed the GPS-based uplift rates and GRACE gravity change solutions in North America and estimated the upper mantle viscosity to be 0.37×10^{21} Pa s and

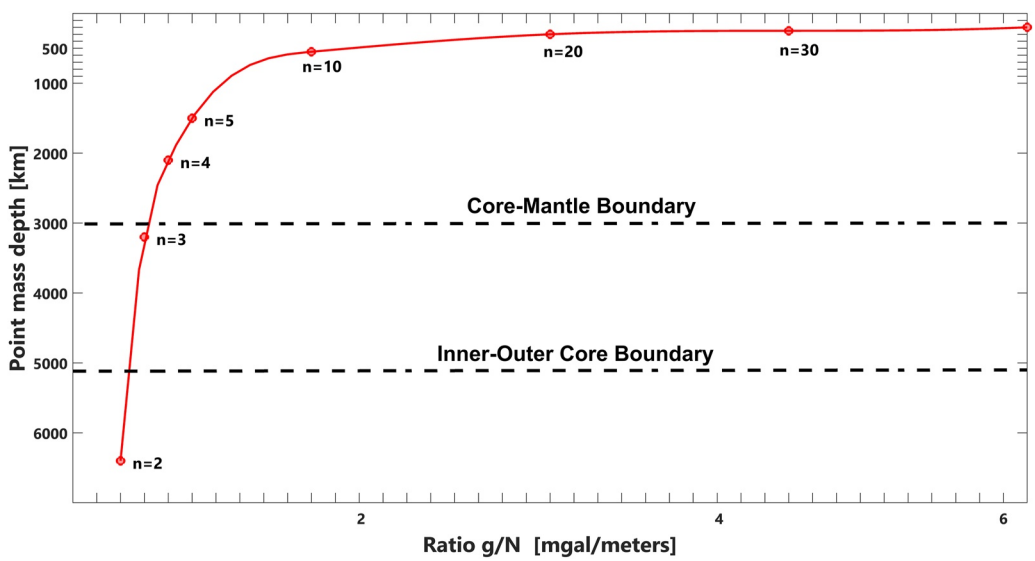

Figure 9. Ratio of gravity to geoid anomalies as a function of depth to a point-mass source. Red circles along the curve show corresponding harmonic degrees (The figure modified after Bowin (2000)).

the lower mantle viscosity to be 1.9×10^{21} Pa s. The Earth model used in Gowan et al. (2016) study for fitting observations has an upper mantle viscosity of 0.4×10^{21} Pa s and a lower mantle viscosity of 10^{22} Pa s. Argus et al. (2021) reported the viscosity of the top 500 km of the lower mantle to be 1.6×10^{21} Pa s (with the mean viscosity of the lower mantle to be 5×10^{21} Pa s) and the upper mantle viscosity to be 0.5×10^{21} Pa s.

Adhikari et al. (2021) discussed that in Greenland, inferred the estimates for the viscosity of the upper mantle are on the order of 0.5×10^{21} Pa s. They reported that the preferred mantle viscosity is in the range of $0.06–0.11 \times 10^{21}$ Pa s, which is 4–8 times smaller than the local upper mantle viscosity reported in Greenland GIA studies (Fleming & Lambeck, 2004; Lecavalier et al., 2014; Simpson et al., 2009).

Below we summarize and compare the obtained results (in this study) with other studies. The previous studies show that the upper mantle viscosity varies between 0.3×10^{21} Pa s and 0.6×10^{21} Pa s, with an average of 0.46×10^{21} Pa s. Similarly, the lower mantle viscosity varies between 1.3×10^{21} Pa s and 13×10^{21} Pa s, with an average of 3.8×10^{21} Pa s. The discrepancy between this study's result and the previous studies can be probably because of several hypotheses and assumptions in developing the procedure (e.g., the equally deformed Earth crust assumption in Sections 3.1 and 3.3). The utilized assumption made the proposed method simpler, but it can affect the uncertainty of the final results. This assumption's reliability will help evaluate the accuracy of the final results. Therefore, the uncertainties of the used land uplift models are different and could affect the obtained viscosities. Table 2 shows that the estimated viscosities are slightly different, and the obtained uncertainties are about one part in 10,000 (varying between 2.6×10^{16} and 1.4×10^{17}). The small magnitude of the obtained uncertainties can be due to some uncertainties are being underestimated or omitted in Equation 11b. In other words, the presented uncertainties reveal the precision of the estimates rather than the accuracies. The accuracies are achievable when all biases in the model are removed correctly. To attain such accuracies, a reasonable way is to avoid the assumption of the equally deformed Earth's crust. However, this practice is hard labor, which is to be conducted in future studies.

The combined land uplift derived from Kalman filtering could cover the discrepancies between the models (see Section 4.2) and give a better solution. For example, the obtained viscosity that is, 7.8×10^{21} and 9.2×10^{21} Pa s in Scenarios 2 and 5, are closer to the one reported by Lambeck et al., 2017 (i.e., 13×10^{21} Pa s) than the other scenarios. Although the results are also close to Caron et al. (2018) that is, 2.3×10^{22} Pa s for the lower mantle viscosity. Different factors can influence the results, such as using correlation analyses to find the best harmonic windows. The reader should be aware that these low correlation coefficients (in Table 2) could be a significant reason for the obtained fluctuating viscosity estimates. In other words, the difference between our results and the results from the methods in the literature could be originated from these low correlation coefficient estimates. Our method is gravimetric analysis-oriented because it relies on the geoid model. Therefore, in finding the relation between the gravity signals (geoid) and the GIA, we encounter some problems, which are: (a) finding the particular part of the gravity field (harmonic) which can sense the present glacio-isostatic relaxation of the Earth, (b) how one can filter out the contribution of other gravitational effects (i.e., contribution due to other mass transportation and deep layers effect). These factors are not easy to model and make the studies more complicated.

5. Conclusion

We inferred the Earth's mantle viscosity from the geoid anomaly and vertical land motions due to the Earth's mass redistribution deglaciation in Greenland. The viscoelastic responses of the Earth's crust (on time scales of a few thousand years) due to deglaciation are important observables to estimate mantle viscosity. In this paper, we used a correlation analysis approach to find the best harmonic window of the geoid (i.e., geoid anomaly that shows the remaining uplift to isostatic equilibrium) so that the truncated geoid reveals maximum correlation with the land uplift rates beneath the Greenland lithosphere. However, the GIA-related gravity field has been mixed with other gravitational signals that can be removed using the proposed approach in this study. We evaluated different land uplift models using pairwise *F*-tests, such as the land uplift obtained from the Greenland Global Positioning System (GPS) Network (GNET), GRACE and the GIA models. The evaluation shows that the uplift rates are different statistically; therefore, one will determine different viscosity values using individual land uplift models. For example, the results showed that the land uplift rates from GRACE and GPS data are similar to the GIA model, which means they statistically belong to the same population. However, the GRACE and GPS data comparison confirms that the discrepancy between them is large. Therefore, a combined land uplift model was

suggested in this study. The Kalman filtering method was applied to estimate a combined land uplift model, which can compensate for the discrepancies. In other words, the land uplift models were combined because the uncertainties of the land uplift models are different in the glaciated regions. Different harmonic windows were obtained by employing different land uplift datasets, for example, the truncated geoid model with a harmonic window between degrees 10 to 39 and 11 to 26 showed a maximum correlation with the GIA model ICE-6G (VM5a) and the combined land uplift rates, respectively. However, we obtained different harmonic windows by employing the vertical displacement rates using GPS and GRACE data. The spatiospectral analysis of the Earth's gravity field helped extract the GIA-related gravity signal by filtering the other effects due to deeper masses that is, core-mantle and shallow layers. Finally, the different land uplift rates together with the GIA-related gravity fields were used to estimate the mantle viscosity. Five scenarios were applied to infer the viscosity beneath the Greenland lithosphere. The result of the combined land uplift model (Scenario 5) is similar to other studies (e.g., Lambeck et al., 2017). The obtained viscosities are between 1.3×10^{21} and 1.9×10^{22} Pa s depending on different radial boundaries in the mantle varying from 200 to 700 km. The proposed method has some advantages with respect to the previous studies. The methodology is more straightforward and consequently faster. In addition, it gives a better picture of the depth interval of the viscosity layer using Bowin (2000) model. However, better estimates are achievable if better GIA models are utilized in the proposed method of this study. More investigations are needed to evaluate the uncertainties of the obtained results that can be done in future studies using different methods for example, ordinary least squares, Bayesian, Monte Carlo, Kalman Filter, etc. However, our study showed the uncertainties of the obtained viscosities, using the propagation of uncertainty method, vary between 2.6×10^{16} and 1.4×10^{17} Pa s.

Appendix A: Statistical Hypothesis Testing

Considering null and alternative hypotheses, one can test the obtained GIA-related vertical land motions statistically. The main idea is to evaluate whether the vertical land motions (VLM) obtained from GRACE, GPS and GIA models belong to the same population or not (i.e., are they equal, or are the differences significant?) To perform this evaluation, one can write null (H_0) and alternative (H_a) hypotheses at for example, $\alpha = 5\%$ significance level:

Case 1:

$$\begin{aligned} H_0 &: \mathrm{VLM_{GRACE}} = \mathrm{VLM_{GIA}} \\ H_a &: \mathrm{VLM_{GRACE}} \neq \mathrm{VLM_{GIA}} \end{aligned} \tag{A1}$$

Case 2:

$$\begin{aligned} H_0 &: \mathrm{VLM_{GRACE}} = \mathrm{VLM_{GPS}} \\ H_a &: \mathrm{VLM_{GRACE}} \neq \mathrm{VLM_{GPS}} \end{aligned} \tag{A2}$$

Case 3:

$$\begin{aligned} H_0 &: \mathrm{VLM_{GPS}} = \mathrm{VLM_{GIA}} \\ H_a &: \mathrm{VLM_{GPS}} \neq \mathrm{VLM_{GIA}} \end{aligned} \tag{A3}$$

The test static can be written

$$z_{obs} = \left| \frac{\mathrm{VLM}_i - \mathrm{VLM}_j}{u(\Delta \mathrm{VLM})} \right| \leq z_{\frac{\alpha}{2}},\ i \text{ and } j = \mathrm{GRACE},\ \mathrm{GPS},\ \text{and GIA} \tag{A4}$$

where

$$u(\Delta \mathrm{VLM}) = \sqrt{u(\mathrm{VLM}_i)^2 + u(\mathrm{VLM}_j)^2} \tag{A5}$$

where $u(\mathrm{VLM}_i)$ and $u(\mathrm{VLM}_j)$ are the uncertainties (error) of the uplift rates obtained by the GRACE, GPS and GIA data. For example, if z_{obs} value is less than $z_{\alpha/2}$, then a hypothesis test at for example, $\alpha = 5\%$ significance level will reject the alternative hypothesis.

Data Availability Statement

The data that support the findings of this study are available from the following sources. The GPS-derived vertical displacement rates obtained from the Greenland Global Positioning System Network (GNET) and provided by https://www.science.org/doi/10.1126/sciadv.1600931. The used GIA models (i.e., Caron et al., 2018 and ICE-6G (VM5a)) were provided by https://vesl.jpl.nasa.gov/solid-earth/gia/ and https://www.atmosp.physics.utoronto.ca/~peltier/data.php. The GRACE RL 05 data were provided by CSR (http://icgem.gfz-potsdam.de/home).

Acknowledgments
We thank the anonymous reviewers and esteemed editor for their careful reading of our manuscript and their many insightful comments and suggestions.

References

Adhikari, S., Caron, L., Milne, G. A., Khan, S. A., Kjeldsen, K. K., Nilsson, J., et al. (2021). Reconciliation of the paleo sea-level record with modern crustal uplift of Greenland. *Earth and Space Science Open Archive M3*. https://doi.org/10.1002/essoar.10507038.1

Amin, H., Bagherbandi, M., & Sjöberg, L. E. (2020). Quantifying barystatic sea-level change from satellite altimetry, GRACE and Argo observations over 2005–2016. *Advances in Space Research*, *65*(8), 1922–1940. https://doi.org/10.1016/j.asr.2020.01.029

Amiri-Simkooei, A. (2007). *Least-Squares estimation of variance components, theory and GPS applications*. Ph.D Thesis. Delft University of Technology.

Argus, D. F., Peltier, W. R., Blewitt, G., & Kreemer, C. (2021). The viscosity of the top third of the lower mantle estimated using GPS, GRACE, and relative sea level measurements of glacial isostatic adjustment. *Journal of Geophysical Research: Solid Earth*, *126*(5), e2020JB021537. https://doi.org/10.1029/2020jb021537

Bagherbandi, M., Tenzer, R., Sjöberg, L. E., & Novák, P. (2013). Improved global crustal thickness modeling based on the VMM isostatic model and non-isostatic gravity correction. *Journal of Geodynamics*, *66*, 25–37. https://doi.org/10.1016/j.jog.2013.01.002

Balling, N. (1980). The land uplift in Fennoscandia, gravity field anomalies and isostasy. *Earth Rheology, Isostasy and Eustasy*, 297–321.

Bjerhammar, A., Stocki, S., & Svensson, L. (1980). *A geodetic determination of viscosity*. Internal report, Division of Geodesy, The Royal Institute of Technology.

Bowin, C. (2000). Mass anomaly structure of the Earth. *Reviews of Geophysics*, *38*(3), 355–387. https://doi.org/10.1029/1999rg000064

Caron, L., Ivins, E. R., Larour, E., Adhikari, S., Nilsson, J., & Blewitt, G. (2018). GIA model statistics for GRACE hydrology, cryosphere, and ocean science. *Geophysical Research Letters*, *45*(5), 2203–2212. https://doi.org/10.1002/2017GL076644

Cathles, L. M., III. (1975). *The viscosity of the earth's mantle* (p. 390). Princeton University Press.

De Geer, G. (1888). Om Skandinaviens nivåförändringar under qvartärperioden. *Geologiska Foreningen i Stockholm Forhandlingar*, *10*(5), 366–379. https://doi.org/10.1080/11035898809444216

Dziewonski, A. M., & Anderson, D. L. (1981). Preliminary reference Earth model. *Physics of the Earth and Planetary Interiors*, *25*(4), 297–356. https://doi.org/10.1016/0031-9201(81)90046-7

Farrell, W. E. (1972). Deformation of the Earth by surface loads. *Reviews of Geophysics*, *10*(3), 761–797. https://doi.org/10.1029/rg010i003p00761

Fleming, K., & Lambeck, K. (2004). Constraints on the Greenland ice sheet since the last glacial maximum from sea-level observations and glacial-rebound models. *Quaternary Science Reviews*, *23*(9–10), 1053–1077. https://doi.org/10.1016/j.quascirev.2003.11.001

Gowan, E. J., Tregoning, P., Purcell, A., Montillet, J.-P., & McClusky, S. (2016). A model of the Western Laurentide Ice Sheet, using observations of glacial isostatic adjustment. *Quaternary Science Reviews*, *139*, 1–16. https://doi.org/10.1016/j.quascirev.2016.03.003

Hager, B. H., & Richards, M. A. (1989). Long-wavelength variations in Earth's geoid: Physical models and dynamical implications. *Philosophical Transactions of the Royal Society of London - Series A: Mathematical and Physical Sciences*, *328*(1599), 309–327. https://doi.org/10.1098/rsta.1989.0038

Haskell, N. A. (1935). The motion of a viscous fluid under a surface load. *Physics*, *6*(8), 265–269. https://doi.org/10.1063/1.1745329

Heiskanen, W. A., & Moritz, H. (1967). *Physical geodesy*. WH Freeman and Company.

Helmert, F. R. (1924). *Die ausgleichrechnung nach der Methode der kleinsten quadrate: Mit anwendungen auf d. Geodäsie, d. Physik ud theorie d. Messinstrumente*. Teubner.

Jentzsch, G. (1997). Earth tides and ocean tidal loading. In *Tidal phenomena* (pp. 145–171). Springer.

Johansson, J. M., Davis, J. L., Scherneck, H., Milne, G. A., Vermeer, M., Mitrovica, J. X., et al. (2002). Continuous GPS measurements of postglacial adjustment in Fennoscandia 1. Geodetic results. *Journal of Geophysical Research*, *107*(B8), 2157. ETG-3. https://doi.org/10.1029/2001jb000400

Joud, S. M. S. (2018). *Contributions of satellite geodesy to post-glacial rebound Research*. KTH Royal Institute of Technology.

Kappelsberger, M. T., Strößenreuther, U., Scheinert, M., Horwath, M., Groh, A., Knöfel, C., et al. (2021). Validation of GIA models in north-east Greenland using densified GNSS measurements and refined estimates of present-day ice-mass changes. In *Copernicus meetings, EGU general assembly 2021*. (EGU21-8019)

Kaufmann, G., & Lambeck, K. (2000). Mantle dynamics, postglacial rebound and the radial viscosity profile. *Physics of the Earth and Planetary Interiors*, *121*(3–4), 301–324. https://doi.org/10.1016/S0031-9201(00)00174-6

Khan, S. A., Sasgen, I., Bevis, M., van Dam, T., Bamber, J. L., Wahr, J., et al. (2016). Geodetic measurements reveal similarities between post–Last Glacial Maximum and present-day mass loss from the Greenland ice sheet. *Science Advances*, *2*(9), e1600931. https://doi.org/10.1126/sciadv.1600931

Kuipers Munneke, P., Ligtenberg, S. R. M., Noël, B. P. Y., Howat, I. M., Box, J. E., Mosley-Thompson, E., et al. (2015). Elevation change of the Greenland Ice Sheet due to surface mass balance and firn processes, 1960–2014. *The Cryosphere*, *9*(6), 2009–2025. https://doi.org/10.5194/tc-9-2009-2015

Kusche, J., & Schrama, E. J. O. (2005). Surface mass redistribution inversion from global GPS deformation and Gravity Recovery and Climate Experiment (GRACE) gravity data. *Journal of Geophysical Research*, *110*(B9). https://doi.org/10.1029/2004jb003556

Lambeck, K., Purcell, A., Zhao, J., & Svensson, N. (2010). The scandinavian ice sheet: From MIS 4 to the end of the last glacial maximum. *Boreas*, *39*(2), 410–435. https://doi.org/10.1111/j.1502-3885.2010.00140.x

Lambeck, K., Purcell, A., & Zhao, S. (2017). The North American Late Wisconsin ice sheet and mantle viscosity from glacial rebound analyses. *Quaternary Science Reviews*, *158*, 172–210. https://doi.org/10.1016/j.quascirev.2016.11.033

Lau, H. C. P., Mitrovica, J. X., Austermann, J., Crawford, O., Al-Attar, D., & Latychev, K. (2016). Inferences of mantle viscosity based on ice age data sets: Radial structure. *Journal of Geophysical Research: Solid Earth*, *121*(10), 6991–7012. https://doi.org/10.1002/2016jb013043

Lecavalier, B. S., Milne, G. A., Simpson, M. J. R., Wake, L., Huybrechts, P., Tarasov, L., et al. (2014). A model of Greenland ice sheet deglaciation constrained by observations of relative sea level and ice extent. *Quaternary Science Reviews*, *102*, 54–84. https://doi.org/10.1016/j.quascirev.2014.07.018

Lidberg, M., Johansson, J. M., Scherneck, H.-G., & Milne, G. A. (2010). Recent results based on continuous GPS observations of the GIA process in Fennoscandia from BIFROST. *Journal of Geodynamics*, *50*(1), 8–18. https://doi.org/10.1016/j.jog.2009.11.010

Ludwigsen, C. A., Khan, S. A., Andersen, O. B., & Marzeion, B. (2020). Vertical land motion from present-day deglaciation in the wider Arctic. *Geophysical Research Letters*, *47*(19), e2020GL088144. https://doi.org/10.1029/2020GL088144

Mishra, D. C., & Kumar, M. R. (2012). Long and short wavelengths of Indian Ocean geoid and gravity lows: Mid-to-upper mantle sources, rapid drift and seismicity of Kachchh and Shillong plateau, India. *Journal of Asian Earth Sciences*, *60*, 212–224. https://doi.org/10.1016/j.jseaes.2012.08.024

Mitrovica, J. X., & Forte, A. M. (2004). A new inference of mantle viscosity based upon joint inversion of convection and glacial isostatic adjustment data. *Earth and Planetary Science Letters*, *225*(1–2), 177–189. https://doi.org/10.1016/j.epsl.2004.06.005

Mitrovica, J. X., & Peltier, W. R. (1991). A complete formalism for the inversion of post-glacial rebound data: Resolving power analysis. *Geophysical Journal International*, *104*(2), 267–288. https://doi.org/10.1111/j.1365-246x.1991.tb02511.x

Niskanen, E. (1949). *On the elastic resistance of the earth's crust*. Isostatic Institute of the International Association of Geodesy.

Olsson, P.-A., Breili, K., Ophaug, V., Steffen, H., Bilker-Koivula, M., Nielsen, E., et al. (2019). Postglacial gravity change in Fennoscandia—Three decades of repeated absolute gravity observations. *Geophysical Journal International*, *217*(2), 1141–1156. https://doi.org/10.1093/gji/ggz054

Paulson, A., Zhong, S., & Wahr, J. (2007). Inference of mantle viscosity from GRACE and relative sea level data. *Geophysical Journal International*, *171*(2), 497–508. https://doi.org/10.1111/j.1365-246x.2007.03556.x

Peltier, R., Argus, D., & Drummond, R. (2013). The new ICE-6G (VM5a) model of the global process of glacial isostatic adjustment. In *EGU general assembly conference abstracts*. EGU2013-6299.

Peltier, W. R. (1974). The impulse response of a Maxwell Earth. *Reviews of Geophysics*, *12*(4), 649–669. https://doi.org/10.1029/rg012i004p00649

Peltier, W. R. (1996). Mantle viscosity and ice-age ice sheet topography. *Science*, *273*(5280), 1359–1364. https://doi.org/10.1126/science.273.5280.1359

Peltier, W. R. (2004). Global glacial isostasy and the surface of the ice-age Earth: The ICE-5G (VM2) model and GRACE. *Annual Review of Earth and Planetary Sciences*, *32*(1), 111–149. https://doi.org/10.1146/annurev.earth.32.082503.144359

Peltier, W. R., & Andrews, J. T. (1976). Glacial-isostatic adjustment—I. The forward problem. *Geophysical Journal International*, *46*(3), 605–646. https://doi.org/10.1111/j.1365-246x.1976.tb01251.x

Peltier, W. R., Argus, D. F., & Drummond, R. (2015). Space geodesy constrains ice age terminal deglaciation: The global ICE-6G_C (VM5a) model. *Journal of Geophysical Research: Solid Earth*, *120*(1), 450–487. https://doi.org/10.1002/2014jb011176

Petrov, L., & Boy, J. (2004). Study of the atmospheric pressure loading signal in very long baseline interferometry observations. *Journal of Geophysical Research*, *109*(B3), B03405. https://doi.org/10.1029/2003jb002500

Rao, C. R. (1971). Estimation of variance and covariance components—MINQUE theory. *Journal of Multivariate Analysis*, *1*(3), 257–275. https://doi.org/10.1016/0047-259x(71)90001-7

Richards, M. A., Hager, B. H., & Sleep, N. H. (1988). Dynamically supported geoid highs over hotspots: Observation and theory. *Journal of Geophysical Research*, *93*(B7), 7690–7708. https://doi.org/10.1029/jb093ib07p07690

Rogozhina, I., Petrunin, A. G., Vaughan, A. P. M., Steinberger, B., Johnson, J. V., Kaban, M. K., et al. (2016). Melting at the base of the Greenland ice sheet explained by Iceland hotspot history. *Nature Geoscience*, *9*(5), 366–369. https://doi.org/10.1038/ngeo2689

Root, B. C., van der Wal, W., Novák, P., Ebbing, J., & Vermeersen, L. L. A. (2015). Glacial isostatic adjustment in the static gravity field of Fennoscandia. *Journal of Geophysical Research: Solid Earth*, *120*(1), 503–518. https://doi.org/10.1002/2014jb011508

Roy, K., & Peltier, W. R. (2017). Space-geodetic and water level gauge constraints on continental uplift and tilting over North America: Regional convergence of the ICE-6G_C (VM5a/VM6) models. *Geophysical Journal International*, *210*(2), 1115–1142. https://doi.org/10.1093/gji/ggx156

Shafiei Joud, M. S., Sjöberg, L. E., & Bagherbandi, M. (2017). Use of GRACE data to detect the present land uplift rate in Fennoscandia. *Geophysical Journal International*, *209*(2), 909–922. https://doi.org/10.1093/gji/ggx063

Simons, M., & Hager, B. H. (1997). Localization of the gravity field and the signature of glacial rebound. *Nature*, *390*(6659), 500–504. https://doi.org/10.1038/37339

Simpson, M. J. R., Milne, G. A., Huybrechts, P., & Long, A. J. (2009). Calibrating a glaciological model of the Greenland ice sheet from the Last Glacial Maximum to present-day using field observations of relative sea level and ice extent. *Quaternary Science Reviews*, *28*(17–18), 1631–1657. https://doi.org/10.1016/j.quascirev.2009.03.004

Sjöberg, L. E. (1983). Unbiased estimation of variance-components in condition adjustment with unknowns-a MINQUE approach. *ZfV*, *108*, 9.

Sjöberg, L. E., & Bagherbandi, M. (2013). A study on the Fennoscandian post-glacial rebound as observed by present-day uplift rates and gravity field model GOCO02S. *Acta Geodaetica et Geophysica*, *48*(3), 317–331. https://doi.org/10.1007/s40328-013-0025-5

Sjöberg, L. E., & Bagherbandi, M. (2017). *Gravity inversion and integration*. Springer.

Spada, G., Ruggieri, G., Sørensen, L. S., Nielsen, K., Melini, D., & Colleoni, F. (2012). Greenland uplift and regional sea level changes from ICESat observations and GIA modelling. *Geophysical Journal International*, *189*(3), 1457–1474. https://doi.org/10.1111/j.1365-246X.2012.05443.x

Svensson, L. (1980). Viscosities from uplifts and geoidal heights. Report. *The Royal Institute of Technology (KTH)* .

Tapley, B. D., Bettadpur, S., Ries, J. C., Thompson, P. F., & Watkins, M. M. (2004). GRACE measurements of mass variability in the Earth system. *Science*, 305(5683), 503–505. https://doi.org/10.1126/science.1099192

Tosi, N., Sabadini, R., Marotta, A. M., & Vermeersen, L. L. A. (2005). Simultaneous inversion for the Earth's mantle viscosity and ice mass imbalance in Antarctica and Greenland. *Journal of Geophysical Research*, *110*(7), 1–14. https://doi.org/10.1029/2004JB003236

Tushingham, A. M., & Peltier, W. R. (1992). Validation of the ICE-3G Model of Würm-Wisconsin Deglaciation using a global data base of relative sea level histories. *Journal of Geophysical Research*, *97*(B3), 3285–3304. https://doi.org/10.1029/91jb02176

van Dam, T., Wahr, J., & Lavallée, D. (2007). A comparison of annual vertical crustal displacements from GPS and Gravity Recovery and Climate Experiment (GRACE) over Europe. *Journal of Geophysical Research*, *112*(B3), B03404. https://doi.org/10.1029/2006jb004335

Wahr, J., Molenaar, M., & Bryan, F. (1998). Time variability of the Earth's gravity field: Hydrological and oceanic effects and their possible detection using GRACE. *Journal of Geophysical Research*, *103*(B12), 30205–30229. https://doi.org/10.1029/98jb02844

Wake, L. M., Lecavalier, B. S., & Bevis, M. (2016). Glacial isostatic adjustment (GIA) in Greenland: A review. *Current Climate Change Reports*, *2*(3), 101–111. https://doi.org/10.1007/s40641-016-0040-z

Walcott, R. I. (1980). Rheological models and observational data of glacio-isostatic rebound. *Earth Rheology, Isostasy and Eustasy*.

Wang, L., Khan, S. A., Bevis, M., van den Broeke, M. R., Kaban, M. K., Thomas, M., & Chen, C. (2019). Downscaling GRACE predictions of the crustal response to the present-day mass changes in Greenland. *Journal of Geophysical Research: Solid Earth*, *124*(5), 5134–5152. https://doi.org/10.1029/2018JB016883

Zhang, L., Tang, H., & Sun, W. (2021). Comparison of GRACE and GNSS seasonal load displacements considering regional averages and discrete points. *Journal of Geophysical Research: Solid Earth*, *126*(8), e2021JB021775. https://doi.org/10.1029/2021jb021775

Zhao, S. (2013). Lithosphere thickness and mantle viscosity estimated from joint inversion of GPS and GRACE-derived radial deformation and gravity rates in North America. *Geophysical Journal International*, *194*(3), 1455–1472. https://doi.org/10.1093/gji/ggt212

Zhao, S., Lambeck, K., & Lidberg, M. (2012). Lithosphere thickness and mantle viscosity inverted from GPS-derived deformation rates in Fennoscandia. *Geophysical Journal International*, *190*(1), 278–292. https://doi.org/10.1111/j.1365-246X.2012.05454.x